Local-Access Model for Proton Transfer in Bacteriorhodopsin[†]

Leonid S. Brown,[‡] Andrei K. Dioumaev,[‡] Richard Needleman,[§] and Janos K. Lanyi*,[‡]

Department of Physiology and Biophysics, University of California, Irvine, California 92697, and Department of Biochemistry, Wayne State University, Detroit, Michigan 48201

Received November 19, 1997; Revised Manuscript Received January 16, 1998

ABSTRACT: The accessibility of the retinal Schiff base in bacteriorhodopsin was studied in the D85N/D96N mutant where the proton acceptor and donor are absent. Protonation and deprotonation of the Schiff base after pH jump without illumination and in the photocycle of the unprotonated Schiff base were measured in the visible and the infrared. Whether access is extracellular (EC) or cytoplasmic (CP) was decided from the effect of millimolar concentrations of azide on the rates of proton transfers. The results, together with earlier work on the wild-type protein, suggest a new hypothesis for the proton-transfer switch: (i) In the metastable 13-*cis*,15-*anti* and *all-trans*,15-*syn* photoproducts, but not in the stable isomeric states, access flickers between the EC and CP directions. (ii) The direction of proton transfer is decided both by this local access and by the presence of a suitable donor or acceptor group (in the wild type), or the proton conductivity in the EC and CP half-channels (in D85N/D96N). (iii) Thermal reisomerization of the retinal can occur only when the Schiff base is protonated, as is well-known. In the wild-type transport cycle, the concurrent local EC and CP access during the lifetime of the metastable 13-*cis*,15-*anti* state enables the changing pK_a's of the proton acceptor and donor to determine the direction of proton transfer. Proton transfer from the Schiff base to Asp-85 in the EC direction is followed by reprotonation by Asp-96 from the CP direction because proton release to the EC surface raises the pK_a of Asp-85 and a large-scale protein conformation change lowers the pK_a of Asp-96. The unexpected finding we report here for D85N/D96N, that when the retinal is in the stable *all-trans*,15-*anti* and 13-*cis*,15-*syn* isomeric forms access of the Schiff base is *locked* (in the EC and CP directions, respectively), suggests that in this protein reisomerization, rather than changes in the proton conductivities of the EC and CP half-channels, provides the switch function. With this mechanism, the various modes of transport reported for Asp-85 mutants (CP to EC direction with blue light, and EC to CP direction with blue *plus* green light) are understood also in terms of rules i−iii.

The requirements for directional ion translocation in transmembrane pumps are conceptually well-defined (*1*−*4*), but little mechanistic information has been available so far, and only for the light-driven proton pump, bacteriorhodopsin. In this protein, the "photocycle" and the ensuing transport of a proton across the membrane are consequences of the photoisomerization of the retinal chromophore (*3*, *5*−*9*). Studies of the intermediate states and their interconversions in the reaction cycle have produced a detailed description of the configurational changes of the retinal and the protein, as well as the proton transfers that add up to the net translocation of a proton from the cytoplasmic (CP)[1] to the extracellular (EC) surface of the membrane. The intermediate states, J, K, L, M, N, and O, and their substates, arise and decay to a large extent in an unbranched sequence after photoisomerization from *all-trans*,15-*anti* to 13-*cis*,15-*anti*. The latter configuration represents an "energized state" of the chromophore, distinct from the 13-*cis*,15-*syn* form[2] (*11*) that is thermally stable and produced slowly in an equilibrium mixture with *all-trans*,15-*anti* during dark-adaptation (*12*, *13*). We illustrate these configurations below (Scheme 1) as well as the *all-trans*,15-*syn* isomer.

Scheme 1

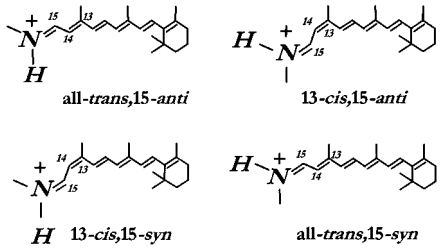

The first proton transfer in the photocycle of the *all-trans*,15-*anti* isomer is from the retinal Schiff base to Asp-85 during the L to M_1 transition. In response to this, a proton is shifted from Glu-204 or water liganded to it (*14*−*18*) to Glu-194 (*19*, *20*), and from there released to the EC surface. This is followed by reprotonation of the Schiff base from Asp-96 in the M_2 to N transition. Asp-96 is reprotonated from the CP surface during the lifetime of N. The retinal reisomerizes to *all-trans* in the N to O transition, and the last step that leads back to the initial state Asp-85 is the

[†] This work was funded partly by grants from the National Institutes of Health (GM 29498 to J.K.L.), the U.S. Department of Energy (DEFG03-86ER13525 to J.K.L.), and the U.S. Army Research Office (DAAL03-92-G-0406 to R.N.).

* To whom correspondence should be addressed.

[‡] University of California.

[§] Wayne State University.

S0006-2960(97)02839-0 CCC: $15.00
Published on Web 02/27/1998

reprotonation of the Glu-204 site.

For active transport across the membrane, these proton transfers must be directional. As in every pump, the connection of the buried proton binding site, in this case the retinal Schiff base, must alternate between the two membrane surfaces during the reaction cycle (*3, 4*). In principle (*8, 21*), the access change may depend entirely on the protein, i.e., on appropriate timing of changes in the ΔpK_a's between the protonated Schiff base and the acceptor and donor groups to its EC and the CP side. In this case, the proton-transfer pathways must be open in both directions while the driving forces vary in magnitude and sign. On the other hand, the access could rely (also) on changes in the local geometry that make and break proton-transfer pathways. In this case, the proton-transfer pathways will alternate between the EC and CP directions, but coordinated with the affinity changes of acceptor and donor. The roles of the changing pK_a's of proton acceptor and donor residues (Asp-85 and Asp-96, respectively) in the directionality of the transport are well established. It is not as clear whether an EC to CP change in the geometry of hydrogen bonds, along which the protons will move, plays an additional role. Such an orientation change would have to occur after the Schiff base deprotonated but before it is reprotonated, i.e., in the step identified as the kinetically observable $M_1 \rightarrow M_2$ reaction (*22, 23*). The objective of this study was to decide the contribution, if any, of local geometry to the protonation switch.

When the proton acceptor and donor are replaced with neutral residues, the protein is simplified. The phenotype of D85N/D96N should reveal if there is an accessibility change that is not dependent on pK_a changes of protein residues but on the isomeric state of the retinal. This mutant is well suited for studies of access for several additional reasons. First, upon replacement of Asp-85 with a nonionic residue, the pK_a of the Schiff base is lowered from >13 to 8−9 (*24*−*27*). This allows investigations of the deprotonation process upon pH jump without illumination, as well as the photoreactions of the unprotonated Schiff base. Second, the D96N mutation makes the CP half-channel very sensitive to azide. Azide acts as a weak acid and facilitates proton exchange between the Schiff base and the bulk (*28*−*31*). Although some degree of proton conduction was seen also in the EC region (*32*), the azide acts at concentrations 2−3 orders of magnitude lower (in the millimolar range) in the CP half-channel (*27, 28, 31*). This influence was virtually absent in the D85N/D96A mutant (*27*), further arguing that the azide affects proton conduction in the CP region where residue 96 is located. In the D85N/D96N mutant, therefore, the direction of access can be probed with azide (*27*). Third, the global protein conformation of D85N/D96N is like that assumed upon deprotonation of the Schiff base in D85N and in the wild-type protein during the photocycle, but independent of the protonation state (*27, 33*). Since this conformation appears to facilitate the proton conductivity of the CP half-channel, in D85N/D96N a change of proton conduction will not complicate the question of access.

From measurements of transient absorption changes in the photocycle of D85N with unprotonated Schiff base, it became known that the Schiff base becomes transiently protonated (*27, 32, 34*). Absorption changes of pH indicator dyes revealed that protons are taken up and released concurrently with the protonation and the subsequent deprotonation, respectively (*34*). Photoelectric measurements had shown that blue-light illumination of D85N and D85N/D96N with unprotonated Schiff base results in continuous proton transport, enhanced in the presence of azide, and in the same CP to EC direction as the wild type (*34, 35*). Simultaneous illumination with blue *and* green light caused proton transport in the opposite direction (*35*). These observations of net proton translocation argued for the existence of an accessibility switch based on a change of local geometry in this process, and suggested that the access to protons might depend directly on the isomeric state of the retinal. When the retinal is *all-trans*,15-*anti*, access would be from the EC side, but when photoisomerized to 13-*cis*,15-*anti* access would change to the CP side (*3*). In the more recent IST model (*9, 36*), the proposed change of access is more complex, as it takes place before proton transfer in some cases and afterward in others. In this model, the access is switched by an unidentified event distinct from either isomerization or proton transfer, and in a "kinetic competition" with the latter. It was suggested that a sequential model (such as in ref *37*) would not account for the transport.

The structure of bacteriorhodopsin is being solved with increasing resolution (*38*−*40*), and a description of the intermediates of the transport cycle at an atomic level seems not far away. In view of this, it is reasonable to ask what actual molecular events decide the direction of proton transfer. In this article, we utilize the D85N/D96N mutant to examine the nature of the access of protons to the Schiff base. The results obtained indicate, unexpectedly, that the access is to the EC direction in the *all-trans*,15-*anti* isomer but to the CP direction in 13-*cis*,15-*syn*. They support the idea that the access is dependent on the isomeric state of the retinal, but not necessarily that it changes from the EC to the CP direction upon photoisomerization from *all-trans*,15-*anti* to 13-*cis*,15-*anti*. Instead, the available evidence suggests that in the metastable photoisomerized state access is open in both EC and CP directions. Accordingly, we propose a mechanism different from other models (*3, 9, 36*). Transport in the wild type is accomplished through the changing affinities of acceptor and donor residues to protons. Transport by D85N mutants, where observed, is according to the same rules but by a mechanism not possible in the wild type, in which recovery of the initial isomeric state with its fixed access can take place before the initial protonation equilibrium is reestablished. "Kinetic competition" between the protonation switch and the proton transfer, as recently postulated (*9, 36*), is not required.

[1] Abbreviations: EC and CP, extracellular and cytoplasmic directions, respectively, relative to the centrally located retinal Schiff base; site-directed mutants are denoted with the residues in the wild type and mutant, separated by the residue number, e.g., D85N/D96N; J, K, L, M, N, and O, intermediates of the bacteriorhodopsin photocycle; FT, Fourier transform; FTIR, Fourier transform infrared; CCCP, carbonyl cyanide *m*-chlorophenyl hydrazone; Bis-tris-propane, 1,3-bis-[[tris(hydroxymethyl)methyl]amino]propane; CAPS, 3-(cyclohexylamino)-1-propanesulfonic acid; MES, 2-(*N*-morpholino)ethanesulfonic acid; CHES, 2-(*N*-cyclohexylamino)ethanesulfonic acid.

[2] The photoproduct of the 13-*cis*,15-*syn* isomer is *all-trans*,15-*syn* (*10*), and under usual conditions its photocycle contains intermediates that do not carry out proton transport.

MATERIALS AND METHODS

Construction of the bacteriorhodopsin mutants D85N and D85N/D96N was previously described (*27*). After their expression in *Halobacterium salinarium*, the proteins were purified as suggested for purple membrane patches (*41*).

Transient absorbance changes at single wavelengths were measured as described earlier (e.g., ref *42*), except that the data were acquired with a 30 MHz analog-to-digital converter (Gage Compuscope 6012/PCI-4M card, Gage Applied Sciences, Montreal, Canada), utilizing custom software. The 4×10^6 data points collected were reductively averaged so as to provide 250 points on a logarithmic time scale. Photoexcitation was with a 420 nm laser pulse, generated with a home-built dye laser (1 mM stilbene in methanol) pumped by a Continuum Surelite II frequency-tripled Nd:YAG laser (Santa Clara, CA). Spectra in photostationary states were determined with an optical multichannel analyzer (*43*) based on a Model TRY700S/B diode array from Princeton Instruments (Trenton, NJ), with illumination provided by a 175 W Cermax xenon lamp (ILC Technology, Sunnyvale, CA).

Measurements of protonation/deprotonation kinetics after a pH jump were measured on a Model SF-61 HiTech stopped-flow sample handling unit (Salisbury, U.K.), with a 2.5 ms mixing time. The same optical arrangement was used as for measuring flash-induced absorption changes in stationary samples. The cation concentrations of samples (except cell envelope vesicles) were kept at 300 mM by using appropriate concentrations of NaCl, NaN_3, and Bis-tris-propane. The initial pH was stabilized with 1 mM Bis-tris-propane. The samples were mixed in a 1:1 ratio with solutions containing 100 mM Bis-tris-propane adjusted to the desired final pH. Where azide was used, it was present at the specified concentration in both solutions. Cell envelope vesicles were in 4 M NaCl, with initially 2 mM buffer. They were mixed with a solution containing 3.3 M NaCl *plus* 0.4 M sodium phosphate, using the stopped-flow instrument described in an earlier publication (*27*). Kinetic data analysis was performed by a nonlinear least-squares global fitting to multiexponentials using the program *FITEXP* (*44*, *45*).

FT-Raman spectra were measured on a Bruker IFS66/S-FRA106/S spectrometer (Bruker Analytische Messtechnik GmbH, Karlsruhe, Germany), as previously described (*33*, *46*). The spectral resolution was 2 cm^{-1}. Sample concentration was about 200 μM. Time-resolved FTIR spectra were measured on a Bruker IFS-66/S spectrometer in the rapid-scan mode, at 4 cm^{-1} resolution. As described elsewhere (*20*), the samples were prepared by drying purple membrane suspensions in distilled water (15−20 nmol of bacteriorhodopsin), at about neutral pH, on a CaF_2 or BaF_2 window (Harrick, Ossining, NY). The semi-dry films, about 15 mm in diameter, were equilibrated with an excess of buffer solution at the desired pH for at least 20 min. They were then partly dried and rehydrated with 3.5 μL of the same buffer, and a second window was placed onto the sample without a spacer.

RESULTS

pK_a of the Protonated Retinal Schiff Base in the D85N and D85N/D96N Mutants, and pH Dependence of the Retinal

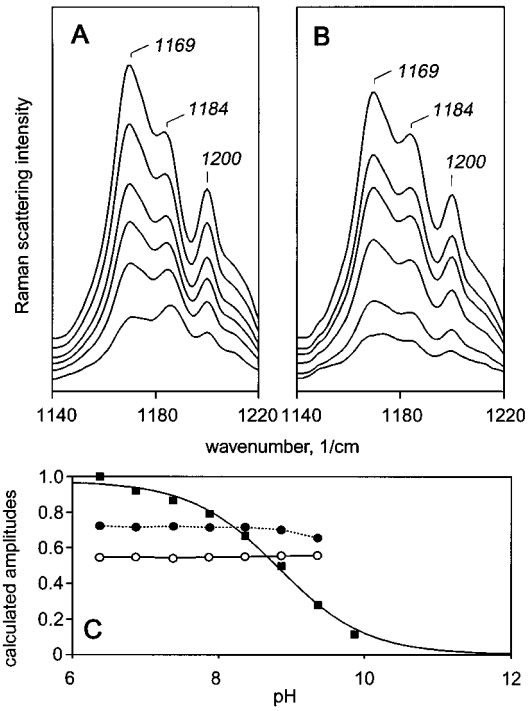

FIGURE 1: FT-Raman spectra of Asp-85 mutants. (A) and (B) show the C−C stretch ("fingerprint") region for D85N and D85N/D96N bacteriorhodopsin mutants, respectively, at various pHs. The pH values, in order of decreasing amplitudes, were 6.4, 7.9, 8.4, 8.9, 9.4, and 9.9. The bands of *all-trans*- (1169 and 1200 cm^{-1}) and *13-cis*-retinal (1184 cm^{-1}) are labeled. (C) shows calculated parameters for D85N/D96N. The *all-trans* content (open circles, solid line) is from the fingerprint region, scaled to the measured *all-trans*-retinal content in D85N (60%) from chemical analysis (*26*) at about pH 6. The fraction of protonated Schiff base (filled squares, solid line), calculated from the combined amplitudes of the ethylenic stretch bands at 1512 and 1528 cm^{-1}, is shown scaled to 1 at the lowest pH. The line is the best fit of the Henderson−Hasselbalch equation with a single protonation equilibrium (pK_a = 8.8, n = 0.72). The filled circles and dashed line show the amplitude of the 1512 cm^{-1} ethylenic stretch band (relative to the sum of the amplitudes at 1512 and 1528 cm^{-1}), attributed to the *all-trans*,15-*anti* configuration (*cf.* text). Conditions: 100 mM NaCl, 10 mM MES, 10 mM Bis-tris-propane, 10 mM CAPS, 22 °C.

Isomeric Composition. FT-Raman spectra measure resonance-enhanced Raman scattering of near-infrared (1064 nm) light (*47*), and the vibrational modes of retinal they contain reveal the isomeric configuration. We had determined FT-Raman spectra for D85N and D85N/D96N near pH 6 and found that they are nearly the same (*33*). The results indicated that, as reported earlier from retinal extraction (*26*, *35*), both mutants contain a mixture of 13-*cis* and *all-trans* forms.

The isomeric compositions of D85N and D85/D96N are illustrated in Figure 1A,B, where the C−C stretch region of the FT-Raman spectra is shown. C−C stretch bands (*48*, *49*) from both 13-*cis*,15-*syn* (1184 cm^{-1}) and *all-trans*,15-*anti* (1169 and 1200 cm^{-1}) isomers are present. Retinal extraction and analysis had shown that the 13-*cis* to *all-trans* ratio for D85N at about pH 6 is 2:3 (*26*, *35*). This is consistent with the relative amplitudes of these bands (*47*). At higher pH, the increased relative amplitude of the 1184 cm^{-1} band and the decreased amplitude of the 1169 and 1200 cm^{-1} bands of D85N (Figure 1A) indicate that the 13-*cis* content becomes markedly higher, also consistent with the data from retinal extraction (*26*). It is evident from Figure 1B, however, that in D85N/D96N the amplitude ratios are

pH independent. The ethylenic stretch bands of D85N/D96N are at 1528 and 1512 cm^{-1} (not shown, but see ref *33*), and correspond to estimated maxima of 570 and 630 nm, respectively in the visible. They must be from the 13-*cis*,15-*syn* and *all-trans*,15-*anti* isomers that are present because earlier results (*50*) have indicated that the spectral shift between *all-trans* and 13-*cis* is large, and may be as much as 70 nm, when the negative charge of the Schiff base counterion is removed. The ratio of these bands is also unaffected by pH (not shown).

The amplitudes of all of these bands become smaller with increasing pH. This reflects the deprotonation of the Schiff base because the yellow chromophore absorbs at a much lower wavelength than the Raman excitation beam, and its bands are strongly attenuated. The ethylenic stretch band of the unprotonated Schiff base can be observed with a small amplitude at 1561 cm^{-1} at the highest pH values used (not shown). The protonation state of the Schiff base is best described from visible spectra, and the deprotonation equilibria measured in that way (*27*) are consistent with the FT-Raman intensities.

The fractional amounts of *all-trans* isomer in the mixtures, as detected in the C−C stretch region, could be calculated by fitting Gaussian curves to the spectra in Figure 1A,B. Corrections were made for the attenuation of the C−C stretch bands that originate from species with blue-shifted absorption maxima by setting the ratios of amplitudes in D85N near pH 6 to the earlier determined 13-*cis* to *all-trans* isomeric ratio of 2:3 (*26*, *35*). The so-calculated decrease in the *all-trans* content in D85N from 60 to 35%, with a pK_a somewhat higher than that of the protonated Schiff base (not shown), agreed with the retinal extraction data where the decrease of *all-trans* content was to 30% (*26*). We note that this agreement holds even though the FT-Raman spectra reflect mostly the isomeric composition of the protonated chromophore while the chemical analyses had determined the retinal content of the entire sample that contained mostly unprotonated Schiff base.[3] Evidently, the protonation state of the Schiff base does not affect the isomeric equilibrium. Figure 1C compares the various measured parameters for D85N/D96N. The fractional amount of *all-trans* isomer from Figure 1B, the relative amplitude of the 1512 cm^{-1} ethylenic stretch band, and the fraction of protonated Schiff base are plotted vs pH. Unlike in D85N, the isomeric composition remains unchanged up to at least pH 9.5, where the Schiff base is significantly deprotonated. The double mutant is unlike D85N also in that the Schiff base deprotonates in a single rather than a biphasic process (*25*), with a pK_a of 8.8 under these conditions, and an N-like purple species of uncertain origin (*25*, *26*, *32*) does not arise when the pH is raised. Complications associated with these properties of D85N are therefore absent in D85N/D96N.

Protonation and Deprotonation of the Schiff Base of the D85N/D96N Mutant Induced by pH Jump. Since the pK_a of the retinal Schiff base in Asp-85 mutants is considerably lower than in the wild type (*24*−*26*), the protonation or deprotonation of the retinylidene group can be induced by a pH jump and its rate determined in a stopped-flow spectrophotometer. We followed the absorption of the protonated Schiff base in membrane patches containing D85N/D96N at 620 nm with better signal/noise than before (*27*). Figure 2A shows traces of absorbance rise upon protonation of the Schiff base after rapid pH decrease from pH 9.0 to 6.5. Azide was added at concentrations between 0 and 2.5 mM in order to distinguish proton access from the EC and the CP surfaces. As illustrated in Figure 2A, the protonation is a multiphasic process, which is particularly evident when azide is added. As the inset to Figure 2A shows, there is one kinetic component that is strongly affected by azide, while the two other components remain slow.

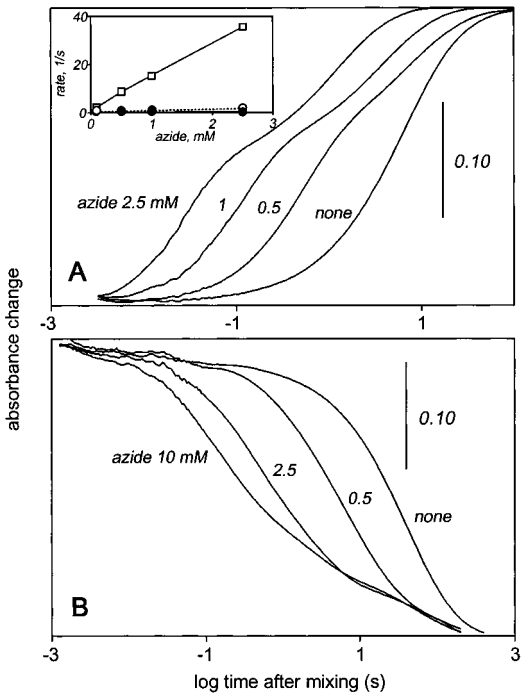

FIGURE 2: Protonation/deprotonation kinetics for the retinal Schiff base in unphotolyzed D85N/D96N. (A) is after rapid pH decrease from 9.0 to 6.5; (B) is after rapid pH increase from 6.5 to 9.0. The absorbance at 620 nm was followed in a stopped-flow spectrometer. Azide concentrations, in order of increasing rates, were 0, 0.5, 1, and 2.5 mM in (A) and 0, 0.5, 2.5, and 10 mM in (B). The inset in (A) shows the rates of the three kinetic components as a function of azide concentration.

Figure 2B shows the same kind of experiment but after a pH increase from 6.5 to 9.0, so as to cause deprotonation of the Schiff base. The azide concentrations used here were between 0 and 10 mM. As in Figure 2A, deprotonation is much more rapid with azide, with slow component(s) that is (are) relatively azide insensitive. The proton equilibration kinetics and the effect of azide indicate therefore that in both protonation and deprotonation two kinds of pathways exist, slow and relatively azide-insensitive ones, as well as a faster azide-responsive ones. From the way azide affects proton conduction in the EC and CP half-channels in other, better described protonation equilibria in the bacterial rhodopsins (*28*−*32*, *52*), we conclude that these pathways are through the EC and the CP half-channels, respectively.

Figure 3A shows absorbance changes after a pH jump similar to that in Figure 2B with 2.5 mM azide, but measured at various wavelengths. The solid lines are the measured traces; the dashed lines are calculated from global fits to

[3] The effects of C_{15}-D substitution in the retinal on resonance Raman bands have suggested that D85N with an unprotonated Schiff base is mostly in the *all-trans* configuration (*51*), but the samples were light-adapted by the Raman laser.

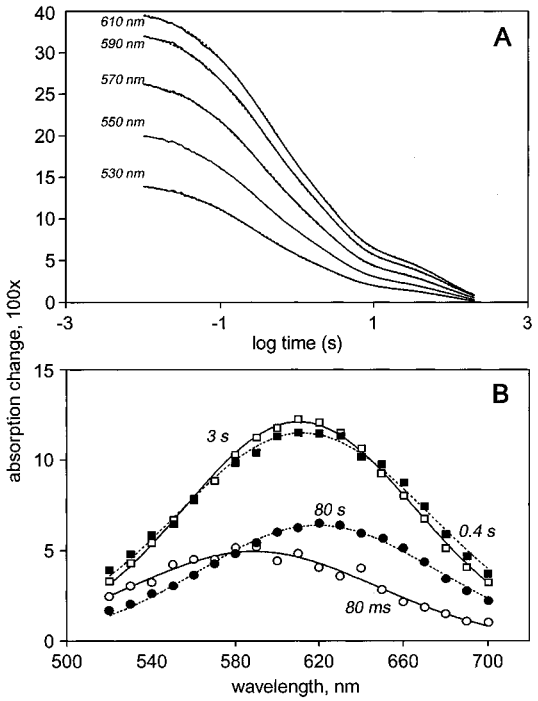

FIGURE 3: Deprotonation kinetics for the retinal Schiff base in D85N/D96N (A), after rapid pH increase from 6.5 to 9.0, and amplitude spectra of the components (B). Absorbance was followed at the indicated wavelengths in a stopped-flow spectrometer as in Figure 2B. Azide concentration was 2.5 mM. The solid lines are the measured traces; the dashed lines are from global fits to data at 19 wavelengths in (B). The time constants and the relative amplitudes of the kinetic components are given in (B). In (B), the amplitudes were fitted with Gaussian curves.

traces at 19 wavelengths. The kinetics are described by at least four kinetic components. Their amplitude spectra are given in Figure 3B. All kinetic components represent depletion of the absorption band, i.e., Schiff base deprotonation that shifts the maximum far to the blue (to near 400 nm). The amplitude spectra show distinct separation of the wavelength maxima. The component with $\tau = 80$ ms appears with a maximum at 590 nm, while the component with a $\tau = 80$ s phase has a maximum at 620 nm. The components with $\tau = 0.4$ and 3 s both appear with maxima at abound 610 nm. It will be shown by infrared spectroscopy (cf. below) that the 620 nm component corresponds to *all-trans*, and the 590 nm component to 13-*cis*, as expected from these maxima. Thus, the fastest component represents deprotonation of mostly the 13-*cis* isomer and the slowest deprotonation of mostly the *all-trans*. The intermediate components appear as mixtures with comparable amounts of both isomers.

Protonation of the Schiff Base in Cell Envelope Vesicles Containing D85N/D96N After a pH Jump. The direction of access was more directly tested by pH jump experiments with cell envelope *vesicles* that contain right-side-out oriented bacteriorhodopsin (*53*). Purple membranes that are open *sheets* served as controls. In the former, protons have direct access to the EC surface, but access to the CP side is only through diffusion across the vesicle membrane. In the latter, proton access is direct in both directions since both membrane surfaces are exposed to the bulk. Figure 4 shows absorption increases at 600 nm, measured in stopped-flow experiments, that reflect protonation of the retinal Schiff base after the pH was rapidly shifted from 9.5 to 6.1. The traces

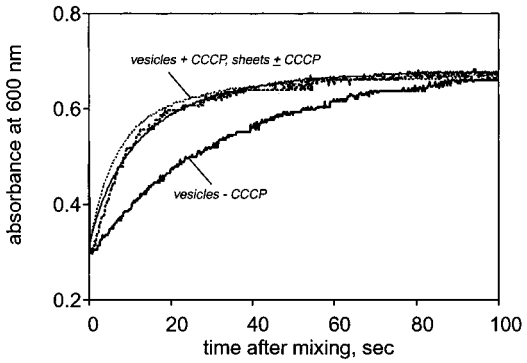

FIGURE 4: Protonation kinetics of the retinal Schiff base of D85N/D96N in cell envelope vesicles and in purple membrane sheets after rapid pH decrease from 9.5 to 6.1. Lines with normal width are traces from the open purple membranes; boldface lines are traces from the closed vesicles. Solid lines are in the absence and dashed lines in the presence of 20 μM protonophore CCCP. The final amplitudes of the traces with the two kinds of preparations were scaled together.

show that the rate of protonation is considerably slower in vesicles than in purple membrane sheets but approaches that in the sheets when the protonophore CCCP is added. The effect of CCCP is minor in the sheets.

If access were entirely from the CP side, the slower rate of Schiff base protonation in the absence of uncoupler would reflect the need for protons to pass across the vesicle membrane. Some degree of access may exist also from the EC side, however. If so, its rate either is slower than through the CP half-channel or reflects a slowly shifting equilibrium toward a conformation in which access is from the EC side. In either case, when the protonophore CCCP is added, it ensures that the faster protonation from the CP side can occur. We conclude from the data in Figure 4, therefore, that (i) protonation of the Schiff base in D85N/D96N is predominantly from the CP surface, and (ii) EC access is not excluded if it is slower, or if the conformation with CP access is intercovertible with another with EC access on a tens of second time scale.

Photocycle of the D85N/D96N Mutant with Initially Unprotonated Schiff Base. When the Schiff base is initially unprotonated, photoexcitation initiates a photocycle in which the Schiff base becomes transiently protonated (*27*, *32*, *34*). This can be followed at alkaline pH by measuring the light-induced absorption change near 600 nm where the protonated, but not the unprotonated, Schiff base absorbs. Figure 5A shows such traces for D85N/D96N. They exhibit complex kinetics strongly dependent on the presence or absence of azide. Protonation of the Schiff base in the absence of azide is slow, as is the deprotonation that follows (both in the 10−100 s time range). Azide, even at concentrations of 10 mM or less, produces dramatic alterations. The rate of protonation increases about 100-fold, and the decay of the protonated state resolves itself into roughly two components, one that is slow and rather azide insensitive, and another that is fast and accelerated nearly 100-fold by azide. Again, the highly azide-sensitive components are attributed to proton transfers through the CP half-channel. The results are thus readily interpreted with the following model. Protonation of the Schiff base after photoexcitation is from the CP side. The deprotonation that follows occurs differently in what appear to be two different populations

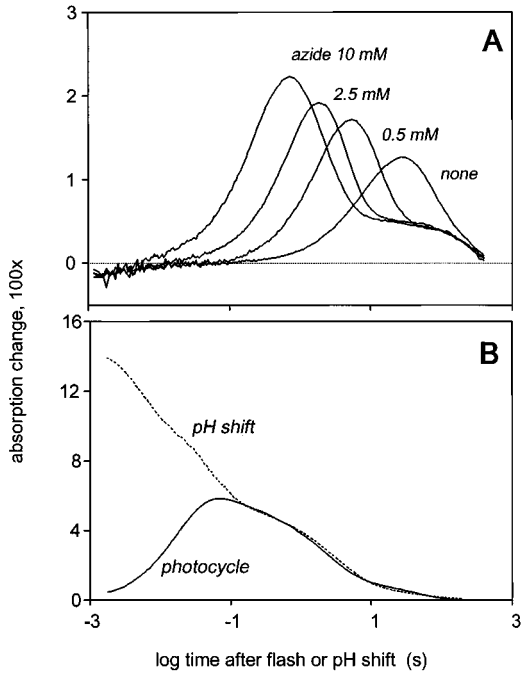

FIGURE 5: Kinetics of the deprotonation and reprotonation of the Schiff base in the photocycle of D85N/D96N with initially unprotonated Schiff base, at various azide concentrations (A), and comparison of the deprotonation kinetics in the photocycle and after a pH jump (B). The absorption change at 620 nm is shown after 420 nm laser pulses in (A), and at 610 nm in (B) after photoexcitation (solid line) and after increasing the pH from 6.5 to 9 (dashed line). Conditions in (A): 0.25 M NaCl, 50 mM Bis-tris-propane, pH 9.0, 24 °C, with azide at the indicated concentrations; in (B); 200 mM azide, 50 mM Bis-tris-propane, pH 9, 20 °C.

(cf. also below). The loss of the Schiff base proton in the photocycle with a slower, azide-insensitive relaxation rate is to the EC side. It can be clearly distinguished from the photocycle with the more rapid and highly azide-sensitive relaxation rate, where the deprotonation is to the CP side.

Figure 5B compares the time course of deprotonation in the photocycle at pH 9 with that induced by pH jump from 6.5 to 9 without illumination. The traces agree remarkably well in the two kinds of experiments. This strongly suggests that by the time the Schiff base begins to deprotonate in the photocycle, the initial conditions of the unilluminated samples, i.e., the thermally stable isomeric mixtures, will have recovered.

The measurements in Figure 5A with 10 mM azide were repeated at various wavelengths (not shown), as in the pH jump experiment with the unphotolyzed protein (Figure 3). In view of the agreement of the photocycle kinetics with the stopped-flow kinetics in Figure 5B, it was not surprising that the results were similar. The fastest deprotonation component observed in the pH jump experiments, with a strongly blue-shifted maximum (Figure 3B), was not seen because the protonation occurred on a slower a time scale. The first observable component, with a time constant of a few seconds, exhibited a maximum at 605 nm, and the slow one at 620 nm, suggesting that they correspond to a mixture of 13-*cis* and *all-trans*, and mostly *all-trans*, respectively. Thus, the results are consistent with the conclusion from the pH jump experiments that the 13-*cis* population deprotonates before the *all-trans*. This possibility was further examined with time-resolved infrared spectroscopy. Figure 6 shows

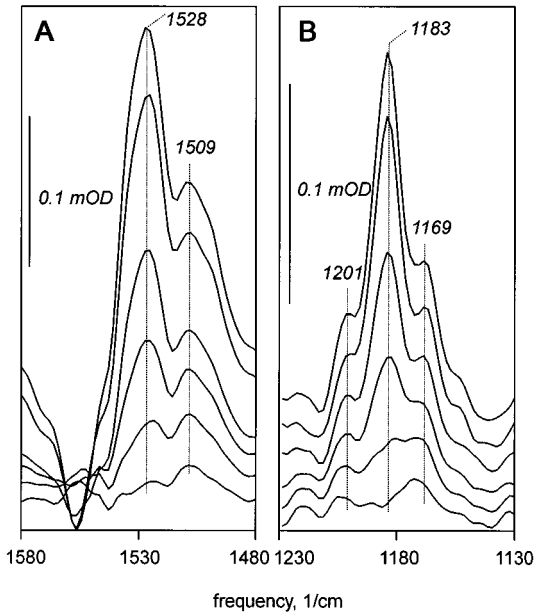

FIGURE 6: FTIR difference spectra for the photocycle of D85N/D96N bacteriorhodopsin with initially unprotonated Schiff base. Difference spectra are shown in the 1480−1580 cm^{-1} region for the C═C stretch bands (A) and in the 1130−1230 cm^{-1} region for the C−C stretch bands (B). The bands discussed in the text are labeled. Delay times after photoexcitation with a 420 nm laser pulse (in the direction of decreasing amplitudes), 0.2, 1, 5, 10, 20, and 30 s. Conditions: 100 mM NaCl, 100 mM phosphate, 100 mM azide, 25 mM CHES, pH 9.5, 5 °C.

FTIR difference spectra at pH 9.5 at various times after photoexcitation with a 420 nm laser pulse. Although the entire midrange infrared frequency region is not shown, the spectra had shapes similar to those determined earlier during continuous illumination of D85N with blue light (*27*, *51*). The two frequency regions shown contain the C═C (ethylenic) stretch and the C−C stretch bands. The infrared vibrational bands of the retinal have very low amplitude when the Schiff base is unprotonated (*54*). Since the depletion bands in Figure 6 are small or entirely absent, the photoreactive species lack a protonated Schiff base as expected. That the difference spectra refer to the photocycle of the unprotonated Schiff base is confirmed also by the small depletion band at 1556 cm^{-1} (Figure 6A) which corresponds to the ethylenic stretch of a species with an absorption maximum near 400 nm, i.e., with an unprotonated Schiff base. All positive bands originate therefore from photointermediate(s) with protonated Schiff base.

The relative amplitudes of the C−C stretch bands indicate that the *all-trans*/13-*cis* ratio changes considerably during the deprotonation of the Schiff base (Figure 6B). The mixture of isomers with protonated Schiff base contains initially mostly 13-*cis* (amplitude at 1183 cm^{-1} dominant over those at 1169 and 1201 cm^{-1}), but during the decay the mixture is considerably enriched in *all-trans* (bands at 1169 and 1201 cm^{-1} gain in amplitude relative to the band at 1183 cm^{-1}). As in the Raman spectra (Figure 1), the two ethylenic stretch bands, at 1509 and 1528 cm^{-1} (Figure 6A), correspond to the *all-trans* and 13-*cis* forms, respectively, and their ratio changes in the same way as the bands in the fingerprint region. The FTIR spectra therefore confirm that the 13-*cis* isomer deprotonates before the *all-trans*.

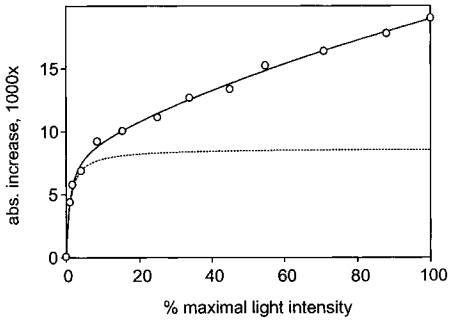

FIGURE 7: Accumulation of the protonated Schiff base in photostationary states at different light intensities in D85N/D96N bacteriorhodopsin. The samples were illuminated through a 350−460 nm filter until a photostationary state was reached, and the spectrum was measured with an optical multichannel analyzer. The absorption increase near 620 nm is plotted vs the relative light intensity. Circles are the measured amplitudes, the solid line is the best fit to a sum of two rectangular hyperbolas (cf. text), and the dashed line is the first of the two components. Half-maximal intensities are 1.1% and 348%. Conditions: same as in Figure 6 but at 22 °C.

Dissection of the Two Photocycles of D85N/D96N with Unprotonated Schiff Base. We suspected from the complexity of the deprotonation kinetics in the pH jump and the photocycle that these samples are heterogeneous and the different protonation rates originate from different populations. The existence of parallel photocycles, and if present the relative rates of the recovery of the initial states in the different populations, can be studied by determining the composition of the photostationary states at different light intensities. The concentration of the photoproduct B in the photoreaction cycle of A will show saturation behavior with respect to light intensity, according to the relationship $[B] = [A^o]/(1 + k_2/k_1)$ where $[A^o]$ is the initial concentration of the unphotolyzed state, [B] is the concentration of the photointermediate at photoequilibrium, and k_1 and k_2 are the rate constants of the photoreaction A → B and the thermal relaxation of B to A, respectively. Each independent photocycle will exhibit a characteristic light intensity at which the intermediate measured accumulates to half of its maximal concentration. If the extinctions and quantum yields of the different populations are the same, the ratios of these half-maximal light intensities will be equal to the ratios of the turnover rates. Figure 7 shows the amplitudes of absorption changes near 610 nm (where maximum increase occurred) as functions of light intensity, measured at high pH in D85N/D96N. It is evident that the data are described by a strongly biphasic saturation curve. Two components, one that saturates at low light intensity (slow photocycle) and another that saturates at high intensity (rapid photocycle), are seen. The ratios of their half-maximal intensities are approximately 330:1. The ratio of the slowest and fastest time constants in the photocycle measurement under the same conditions was about 400:1. Thus, at least some of the kinetic complexity in the deprotonation of the Schiff base originates from the existence of two parallel photocycles.

DISCUSSION

The D85N/D96N mutant lacks a proton acceptor and a donor, and the observation of various modes of transport in this protein and other Asp-85 mutants argued (*9, 35, 36*) that the reactions of the retinal Schiff base are sufficient to accomplish proton translocation. How does such transport occur, and what is its relevance for transport in the wild type? We report here on the photoreaction cycle of D85N/D96N with initially unprotonated Schiff base, with particular attention to the directionality of the transient proton transfers that ensue, and compare the findings with results for the unphotolyzed protein where the protonation equilibria were measured after a pH jump.

In the photocycle of the species with unprotonated Schiff base, as well as in the pH jump experiments, the protonation/deprotonation kinetics of the Schiff base are unexpectedly complex, and suggest a heterogeneous population. The dependence of the photostationary state on light intensity (Figure 7) confirms that a heterogeneity exists, and that one of the two populations exhibits more rapid deprotonation kinetics than the other. The most obvious candidate for the heterogeneity is the isomeric configuration, since the chromophore of D85N/D96N does in fact contain a mixture of *all-trans*,15-*anti*- and 13-*cis*,15-*syn* retinal (Figure 1). In D85N, the two isomers had been shown (*26*) to undergo thermal interconversion only on the time scale of the proton exchange reactions of the Schiff base (about 1 min). The correspondence of the ratio of the deprotonation rates in the photostationary experiments for the two populations (Figure 7) with the ratio of the deprotonation rates for 13-*cis* and *all-trans* in single-turnover experiments (and with the general observation that 13-*cis* deprotonates more rapidly than *all-trans*) confirms that the heterogeneity resides in the isomeric states. According to the results we report, the rates of proton exchange and the direction of access of protons are different for the two isomers, and this is what produces the observed kinetic components.

The absorption maxima in the visible (Figure 3B) and the FTIR spectra (Figure 6) indicate that the 13-*cis*,15-*syn* isomer deprotonates first and the *all-trans*,15-*anti* last. The strong effect of azide on the faster of the protonation and deprotonation processes (Figures 2 and 5A) suggests that these occur through the CP half-channel. That access to the CP surface is faster than access to the EC surface is demonstrated directly by the experiments with envelope vesicles (Figure 4). The relative insensitivity of the slower protonation/deprotonation processes to azide (Figures 2A and 5A) suggests, in turn, that these occur through the EC half-channel. Interestingly, therefore, these observations link the 13-*cis*,15-*syn* isomer to proton transfer in the CP direction, and the *all-trans*,15-*anti* to proton transfer in the EC direction. Such a difference in the connection of the Schiff base nitrogen to proton conducting groups between the two thermally stable isomeric states is entirely unexpected because in the 13-*cis*,15-*syn* state the additional, $C_{15}-N$ bond rotation will have reoriented the Schiff base to roughly the same direction it faces in the *all-trans*,15-*anti* configuration (*10, 55*). In any case, one would not expect that an access change based on the slow thermal interconversion between the two stable isomeric states could have a role in transport.

The same kind of argument suggests, however, that the strongly azide-sensitive protonation process in the photocycle of the unprotonated Schiff base (Figure 5A) is from the CP side. Although the 13-*cis*,15-*syn* and *all-trans*,15-*anti* forms have independent photocycles (Figure 7), this will be true for both. The near-identity of the deprotonation kinetics in the photocycle to those observed upon pH jump with

unilluminated samples (Figure 5B) indicates that the deprotonation occurs only after the initial thermally stable isomeric states have recovered. This is what allows the possibility of transport by D85N/D96N. Since the proton access in the *all-trans*,15-*anti* configuration is necessarily to the EC side, recovery of this state in the photocycle of the *all-trans* form before deprotonation will allow the release of the Schiff base proton, received from the CP side, to the EC surface. The effectiveness of this transport cycle will be somewhat diminished by any (slow) thermal equilibration of the reisomerized *all-trans*,15-*anti* state with 13-*cis*,15-*syn* during the deprotonation, since access in the latter state is to the CP side. Little transport is expected from the photocycle of the 13-*cis*,15-*syn* form since after recovery of the initial isomeric state the access will be in the CP direction. Access to the EC side could be gained only by thermal equilibration of the recovered 13-*cis*,15-*syn* isomer with *all-trans*,15-*anti*, and this will not compete with the more rapid relaxation through the CP side. In 13-*cis* photocycle, therefore, the Schiff base proton will be released mostly through the same pathway as its uptake.

The rapid deprotonation in the CP direction will deplete the 13-*cis*,15-*syn* isomer formed directly by reisomerization from *all-trans*,15-*syn* in the photocycle of the 13-*cis* form and indirectly (and more slowly) by isomeric equilibration from *all-trans*,15-*anti* in the photocycle of the *all-trans* form. Thus, the fraction that deprotonates early will appear to be mostly 13-*cis*, and the fraction that deprotonates last will be mostly *all-trans* (Figure 6). Kinetic components with rates intermediate between the two, that proved to be mixtures of 13-*cis* and *all-trans*, arise probably through slow thermal interconversion of the isomeric states during the deprotonation.

That the recovery of the initial isomeric states occurs before deprotonation of the Schiff base can be understood from the influence of the protonated state of the Schiff base on the barriers to bond rotations in the retinal. Quantum chemical calculations had shown that the C=C bond order is higher and therefore isomerization around the $C_{13}-C_{14}$ bond is slower when the Schiff base is unprotonated (*56, 57*). In the wild-type photocycle, the retinal remains trapped in the 13-*cis*,15-*anti* isomeric configuration as long as the Schiff base is deprotonated (in the M intermediate). Thus, thermal recovery of the initial state can be only from the protonated intermediates that follow (the N and O states). In contrast, during the photocycle of the initially unprotonated Schiff base, there is no such barrier to reisomerization because the intermediate contains a protonated Schiff base. Reisomerization is rapid, and the slow recovery of the unprotonated state of the Schiff base is from the initial isomeric forms.

Can a Change of the Isomeric Configuration of Retinal Account for the Change of Proton Access? It would be tempting to conclude from these observations that proton transport in D85N/D96N is by a mechanism in which the access of the Schiff base simply changes from the EC to the CP direction when the retinal is photoisomerized from *all-trans*,15-*anti* to 13-*cis*,15-*anti*. Since we find that the stable *all-trans*,15-*anti* and the 13-*cis*,15-*syn* isomeric forms have different directions of access, an isomeric configuration dependent access change seems reasonable, and this mechanism had been proposed before (*3, 51*). However, such a model is seriously contradicted by the events in the photocycle of the wild-type protein. The Schiff base transfers its proton to Asp-85 (to the EC side) and receives a proton from Asp-96 (from the CP side) while in the 13-*cis*,15-*anti* isomeric state throughout (*58*−*60*). Reisomerization to *all-trans*,15-*anti* occurs much later in the photocycle (*61*). A possible solution would be access change upon a second isomerization of the retinal: a rotation of the $C_{14}-C_{15}$ single bond after deprotonation of the Schiff base (*62*). However, Raman spectra rule out such a configurational change (*58, 59*). The recently proposed IST model (*9, 36*) overcame this problem by postulating a switch event ("S") defined only by its property that it is distinct from the retinal isomerization ("I") and independent from the proton transfer ("T"). In the wild type, but not in Asp-85 mutants, S was assumed to be delayed relative to I. Depending on conditions, the switch S could now occur either before or after T. This explained the observation of transport in the CP to EC direction upon blue-light illumination, and in the reverse direction in the two-photon reaction of D85N and D85N/D96N (*35*), as well as proton transport by sensory rhodopsin I in the absence of transducing protein (*63*−*67*). It was invoked (*36*) to explain also the binding (*68*) and EC to CP transport (*36, 69*) of chloride in the D85T mutant. The change of proton access therefore requires an unidentified structural rearrangement of the retinal or the protein, and would occur under some conditions immediately upon isomerization while under others delayed by as much as several milliseconds in a "kinetic competition" between S and T.

It should be clear from this that elucidating the general mechanism of the protonation switch depends on being able to successfully reconcile the properties of the Asp-85 mutants, described earlier (*27, 34, 35, 51*) and reported here, with the wild type. In the next section, we describe, therefore, what is known about the accessibility of protons in the wild-type photocycle.

Access in the Photocycle of the Wild-Type Protein. From a large variety of experimental approaches, that include spectral and kinetic analyses of the photocycle (*22, 23, 70, 71*), blue-light photoreaction of the M intermediate as followed in the visible (*72*) and in the infrared (*73*) and by photoelectric measurements (*74*), FTIR spectra (*75*), and X-ray diffraction (*76*−*80*), the M state with a deprotonated Schiff base could be resolved into an early substate, M_1, and a late substate, M_2. As anticipated (*81*−*83*), the kinetics confirmed that *the protonation equilibrium of the Schiff base is with Asp-85 in M_1, but with Asp-96 in M_2* (*22, 23*). The $M_1 \rightarrow M_2$ reaction appeared unidirectional at the available signal/noise ratio at pH $\geq$7 (*22, 71*). The irreversibility is a result of the coupling of the pK_a of Asp-85 to the protonation state of the proton release site (*15, 18, 84*). When the pH is above the pK_a for proton release (about 6), free energy is dissipated, the pK_a of Asp-85 rises, and the protonation equilibrium shifts toward nearly full deprotonation of the Schiff base. Importantly, however, the M_1 to M_2 reaction is reversible at pH <6, where proton release to the EC surface does not occur. According to the calculated rate constants (*71*), the equilibrium constant $K = [M_2]/[M_1]$ is 20, indicating that the transition to M_2 includes additional dissipation of free energy independent of proton release. Nevertheless, since the equilibrium of L and M_1 favors L by a factor of about 4 (*71*), at pH <6 the L state persists to a readily

measured extent until recovery of the initial state. This indicates that M_1 and M_2 remain in equilibrium, and the Schiff base retains its connection with both Asp-85 and Asp-96. In mutants where either the $M_1 \Leftrightarrow M_2$ (*71*) or the $L \Leftrightarrow M_1$ (*85*) equilibrium lies further toward the back-reaction, the concentration of L is greater and even dominant over M at pH <6. Evidently, unless the proton release to the EC surface raises the pK_a of Asp-85, access of the Schiff base at this time in the photocycle is to both directions concurrently. The effects of external electric field on proton transport (*86*) also indicate that such an equilibrium exists, and that it is linked to an electrogenic event. Molecular dynamics calculations (*87*) confirm that in the 13-*cis*,15-*anti* photoproduct of the wild-type protein access is feasible in both EC and CP directions. Concurrent access would be accomplished if the connection of the Schiff base to the two proton conduction pathways flickered rapidly (with the time constant of the $M_1 \Leftrightarrow M_2$ equilibration, i.e., 30 μs) so as to allow proton transfer in either direction. The pump is not stalled at low pH, or in mutants where proton release is blocked, however. The correct directionality of the proton flux under these conditions is enforced by the fact that recovery of the initial state is (largely) impossible from the L intermediate, and the equilibrium is ultimately drawn in the direction of CP access.

The "Local-Access" Mechanism of the Protonation Switch. In the following, we describe a general mechanism for the protonation switch, suggested by the experimental evidence on proton access in D85N/D96N we report here and the earlier findings of its various transport modes (*9, 35, 36*), and the wild-type photocycle. This mechanism contains the following elements. (i) In the 13-*cis*,15-*anti* and *all-trans*,15-*syn* metastable isomeric states produced by illumination from the *all-trans*,15-*anti* and 13-*cis*,15-*syn* initial states, respectively, the access of the Schiff base is concurrently to both EC and CP directions. This lack of fixed direction may occur because when the Schiff base is displaced from its position in the stable states some degree of steric conflict with the protein matrix could allow rapid fluctuation, "flickering," of the local geometry. (ii) The direction of proton transfer to either membrane surface during the lifetime of the metastable isomeric configurations is determined by factors inherent in the protein (*58, 59*), i.e., the pK_a's of the donor and acceptor groups or the rate of proton conduction in the two-half-channels. (iii) The barrier to thermal reisomerization is high when the Schiff base is unprotonated (*56, 57*), and thus thermal reisomerization occurs in the photocycles only while the Schiff base is protonated. (iv) Under physiological conditions, proton conduction cannot be rapid *simultaneously* to both EC and CP surfaces. Thus, the protein will not passively dissipate a proton gradient to a significant extent, either in the dark or during illumination. (v) The direction of access is locked entirely in one direction in the stable *all-trans*,15-*anti* and 13-*cis*,15-*syn* forms, in the EC direction in the former and the CP direction in the latter. This unexpected outcome of our study of D85N/D96N allows interpretation of the photocycle of transport by Asp-85 mutants in the same terms as the wild type. (vi) *There is no kinetic competition between the protonation switch and proton transfer*, such as postulated recently (*9, 36*). These elements produce the following mechanistic schemes for the various photocycles and transport modes observed. For simplicity, the models include only those photointermediates relevant to proton transfer and their changing directions.

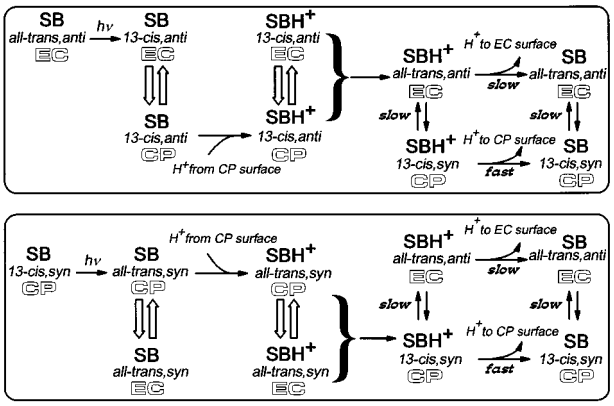

FIGURE 8: Proposed scheme for the photocycle of D85N/D96N with *all-trans*,15-*anti*- and 13-*cis*,15-*syn*-retinal, and initially unprotonated Schiff base (*cf.* discussion in the text).

Photocycle of the all-trans,15-anti and 13-cis,15-syn Forms of D85N/D96N with Unprotonated Schiff Base. Figure 8 shows a scheme in which the access of the Schiff base is in the EC direction when the retinal is *all-trans*,15-*anti*, but in the CP direction when 13-*cis*,15-*syn*. In both metastable 13-*cis*,15-*anti* and *all-trans*,15-*syn* photoproducts, an equilibrium between EC and CP access develops (wide arrows). Although the local geometry at the Schiff base would allow it, proton conduction through the EC half-channel is slow and does not compete with CP access. It is omitted from the scheme. Protonation is therefore decisively from the CP side. Reisomerization to *all-trans*,15-*anti* in the *all-trans* photocycle causes recovery of EC access, and the Schiff base proton is lost perforce to the EC side. This results in net translocation of a proton. Thermal equilibration with the 13-*cis*,15-*syn* configuration (dark adaptation), that allows access also in the CP direction, is a competing pathway of relaxation that should decrease transport because the CP half-channel will conduct protons rapidly in the presence of even low concentrations of azide. On the other hand, to a smaller extent will azide accelerate proton transfer in the EC direction also (*32*), and thus increase transport (*35*). We note that since it is in the EC region, this effect of azide should be seen also in D85N.

At the end of the 13-*cis* photocycle (Figure 8), recovery of the reisomerized 13-*cis*,15-*syn* state results in access to the CP direction. Proton equilibration with the EC side would be possible only through thermal equilibration of the 13-*cis*,15-*syn* form with the *all-trans*,15-*anti*. Because the Schiff base proton is lost more rapidly to the CP side, such thermal isomerization to *all-trans* and therefore EC access will be negligible. In this case, CP access returns the proton gained from the same side earlier in the cycle, and little net transport can occur.

In the following, we extend the mechanism in Scheme 1 and in Figure 8 to other photoreactions of Asp-85 mutants in which transport was tested (*9, 35, 36, 69, 88*), and to the wild type.

Photocycle of D85N and D85N/D96N during Simultaneous Illumination with Blue and Green Light. Photoisomerization of the *all-trans*,15-*anti* isomer of Asp-85 mutants to 13-*cis*,15-*anti* during illumination with green light will produce a changed local geometry, and a rapid equilibrium between

local conformations with accessibilities in the EC and CP directions. Deprotonation of the initially protonated Schiff base is toward the CP side because proton conduction in the EC region is slow and competes ineffectively with deprotonation to the CP direction (Figure 8 and ref *27*). Simulation of the structure of the 13-*cis*,15-*anti* state suggested that in this photocycle the D85N mutation limits local access toward the EC half-channel by reorienting the Schiff base in the CP direction (*87*). This would give the same result although by a different mechanism. The protonation equilibrium of the Schiff base is in a side reaction (*27*), and little or no transport can result,[4] as reported (*35*). Continuous green-light illumination of D85N and D85N/D96N will cause accumulation of the intermediate with deprotonated Schiff base. This intermediate can undergo a secondary photoreaction if blue light (the absorption maximum of this yellow chromophore is near 410 nm) is provided simultaneously. The resulting photoreisomerization to *all-trans*,15-*anti* recovers access of the Schiff base exclusively to the EC direction, and the proton is regained from this side. This two-photon reaction cycle will result therefore in the net translocation of a proton, but in the reverse direction from the wild type, from the EC to the CP side, as reported (*35*).

Chloride Transport in D85T Bacteriorhodopsin and Halorhodopsin. The binding of protons in the bacteriorhodopsin transport cycle is mainly to aspartate and glutamate residues, and chloride binding is observed only under special circumstances (*89*−*92*) or in mutants (*68, 93*). It is therefore likely that the pathways of proton transport in bacteriorhodopsin are different from those of chloride transport in halorhodopsin. The molecular details of the local access of protons and chloride at the active site, and their changes, are likely to be different also. Nevertheless, since the D85T mutant transports chloride, and in the EC to CP direction like halorhodopsin (*9, 36, 69*), any general mechanism of proton transport should allow for the translocation of anions and for the reversal of its direction. It is worth noting, therefore, that the mechanism we propose here is not specific for transport in either EC or CP direction. Access being available in both directions during the lifetime of the photoisomerized state, the direction of transport depends on the functional opening and closing of the EC and CP half-channels and/or the availability of binding sites with suitable affinities. If the structure of unphotolyzed halorhodopsin (*94*) resembles the conformation of the M and N photointermediates in bacteriorhodopsin as we had suggested (*95*), it is possible that the conformational shift could occur in the opposite direction upon illumination, and that the ensuing changes in the two half-channels could move chloride from the EC to CP direction.

Photocycle of the all-trans,15-anti Isomeric Form of the Wild-Type Protein. Figure 9 shows the wild-type photocycle in the same terms as in Figure 8. If the local geometry of the active site in the wild-type protein is like in D85N/D96N, the access of the Schiff base in the initial *all-trans*,15-*anti* isomer will be in the EC direction. However, this plays little role in the transport. Once in the L state, the local access flickers rapidly between EC and CP. Asp-96 to the CP side

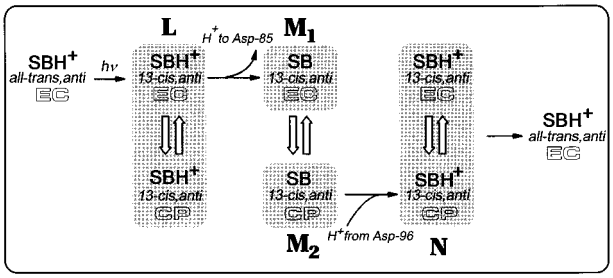

FIGURE 9: Proposed scheme for the photocycle of wild-type bacteriorhodopsin with *all-trans*,15-*anti*-retinal (*cf.* discussion in the text).

is protonated and cannot be a proton acceptor. For reasons that have to do with the changed geometry at the Schiff base upon photoisomerization (*85, 96*), and possibly changes in liganded water (*97*), Asp-85 to the EC side becomes a proton acceptor. Thus, the Schiff base proton is transferred in the EC direction, and thereby generates M_1. The access of the unprotonated Schiff base continues to flicker between the EC and CP directions (as implied by the $M_1 \leftrightarrow M_2$ equilibrium). At this time, the protonation pathway changes from the EC to the CP direction. This is initiated by release of a proton from the EC surface that further raises the pK_a of Asp-85 (*15, 18, 84*) and makes it unavailable as a proton donor to the Schiff base. Continued proton exchange with the EC side is thus excluded. A large-scale protein conformation change (*76, 77, 80, 98*−*101*) lowers the pK_a of Asp-96, and probably increases proton permeability of the CP region (*42, 102, 103*). This makes a proton available from the CP side. Reprotonation of the Schiff base, that produces the N intermediate, occurs therefore in M_2 and from Asp-96.

Thus, in this mechanism the isomeric states of the retinal and the acceptor and donor groups of the protein have different and well-defined functions. The EC to CP switch does not reside in the retinal isomeric states. Instead, the flickering local access in the metastable photoisomerized state *enables* the changing proton affinities, that allow proton conduction in the EC and CP half-channels, to decide the direction of the transfers. The switch is therefore furnished by the protein as suggested earlier (*58*), but requires configurational change of the retinal at the active site. Although the acceptor and donor groups in the protein utilize the accessibilities for proton transfer only in M_1 and M_2, local access of the Schiff base is predicted to remain open in both EC and CP directions for all intermediates that contain 13-*cis*,15-*anti*-retinal. Indeed, in the case of the L intermediate, there is evidence for structural changes in both EC and CP regions. The hydrogen-bonding changes of bound water in the EC region, and the perturbation of the peptide backbone, various residues, as well as bound water, in the CP region, detected by FTIR spectroscopy (reviewed in ref *104*), may reflect the simultaneous connection of the positively charged protonated Schiff base to both EC and CP half-channels.

CONCLUSIONS

The protonation switch, considered before as a concept, is now mechanistically explicit. It is embodied entirely in (i) the isomerization step (local access) and (ii) the proton-transfer step (proton conduction to and from the active site).

[4] Proton transport by the D85T mutant (*9, 36*) suggests that unlike asparagine, threonine at position 85 allows significant proton conduction in the EC region.

The observed mechanisms of transport modes illustrate the distinction between these two essential components. In general terms, *local geometry at the active site* is firmly locked in one direction in the stable initial state, but flickers rapidly between the two alternative directions in the metastable intermediate state. The resulting access to both EC and CP directions enables the *donor and acceptor groups (or proton conduction pathways) furnished by the protein* to add or remove a proton from the active site during the lifetime of the intermediate states. Thus, in the wild-type protein, the orderly changes in the pK_a's of these groups, caused by secondary events in the reaction cycle such as proton release to the surface and a large-scale conformational change, bring about unidirectional CP to EC proton translocation, while local access remains unchanged. When the proton acceptor and donor are missing (e.g., in the D85N/D96N mutant), the same principles apply, but the mechanism is different. Proton conduction in the EC direction is now considerably less than in the CP direction. Where transport is observed, it is always the result of the fact that the CP access to the surface, which is dominant over EC access during the lifetime of the intermediate state, is followed by recovery of the initial local geometry, and thus obligatory EC access, before the proton reequilibration. Unlike in the wild-type transport cycle, the proton conductivities in the two half-channels remain constant and the local access is what changes.

REFERENCES

1. Jencks, W. P. (1980) *Adv. Enzymol. 51*, 75−106.
2. Tanford, C. (1983) *Annu. Rev. Biochem. 52*, 379−409.
3. Oesterhelt, D., Tittor, J., and Bamberg, E. (1992) *J. Bioenerg. Biomembr. 24*, 181−191.
4. Lanyi, J. K. (1995) *Nature 375*, 461−463.
5. Mathies, R. A., Lin, S. W., Ames, J. B., and Pollard, W. T. (1991) *Annu. Rev. Biophys. Biophys. Chem. 20*, 491−518.
6. Rothschild, K. J. (1992) *J. Bioenerg. Biomembr. 24*, 147−167.
7. Ebrey, T. G. (1993) in *Thermodynamics of membranes, receptors and channels* (Jackson, M., Ed.) pp 353−387, CRC Press, New York.
8. Lanyi, J. K. (1993) *Biochim. Biophys. Acta 1183*, 241−261.
9. Haupts, U., Tittor, J., Bamberg, E., and Oesterhelt, D. (1997) *Biochemistry 36*, 2−7.
10. Logunov, I., Humphrey, W., Schulten, K., and Sheves, M. (1995) *Biophys. J. 68*, 1270−1282.
11. Harbison, G. S., Smith, S. O., Pardoen, J. A., Winkel, C., Lugtenburg, J., Herzfeld, J., Mathies, R. A., and Griffin, R. G. (1984) *Proc. Natl. Acad. Sci. U.S.A. 81*, 1706−1709.
12. Sperling, W., Carl, P., Rafferty, C. N., and Dencher, N. A. (1977) *Biophys. Struct. Mech. 3*, 79−94.
13. Aton, B., Doukas, A. G., Callender, R. H., Becher, B., and Ebrey, T. G. (1979) *Biochim. Biophys. Acta 576*, 424−428.
14. Brown, L. S., Sasaki, J., Kandori, H., Maeda, A., Needleman, R., and Lanyi, J. K. (1995a) *J. Biol. Chem. 270*, 27122−27126.
15. Richter, H. T., Brown, L. S., Needleman, R., and Lanyi, J. K. (1996) *Biochemistry 35*, 4054−4062.
16. Richter, H. T., Needleman, R., and Lanyi, J. K. (1996) *Biophys. J. 71*, 3392−3398.
17. Sampogna, R. V., and Honig, B. (1996) *Biophys. J. 71*, 1165−1171.
18. Balashov, S. P., Imasheva, E. S., Govindjee, R., and Ebrey, T. G. (1996) *Biophys. J. 70*, 473−481.
19. Balashov, S. P., Imasheva, E. S., Ebrey, T. G., Chen, N., Menick, D. R., and Crouch, R. K. (1997) *Biochemistry 36*, 8671−8676.
20. Dioumaev, A. K., Richter, H. T., Brown, L. S., Tanio, M., Tuzi, S., Saitô, H., Kimura, Y., Needleman, R., and Lanyi, J. K. (1998) *Biochemistry* (in press).
21. Kalisky, O., Ottolenghi, M., Honig, B., and Korenstein, R. (1981) *Biochemistry 20*, 649−655.
22. Váró, G., and Lanyi, J. K. (1991) *Biochemistry 30*, 5008−5015.
23. Váró, G., and Lanyi, J. K. (1991) *Biochemistry 30*, 5016−5022.
24. Otto, H., Marti, T., Holz, M., Mogi, T., Stern, L. J., Engel, F., Khorana, H. G., and Heyn, M. P. (1990) *Proc. Natl. Acad. Sci. U.S.A. 87*, 1018−1022.
25. Brown, L. S., Bonet, L., Needleman, R., and Lanyi, J. K. (1993) *Biophys. J. 65*, 124−130.
26. Turner, G. J., Miercke, L. J. W., Thorgeirsson, T. E., Kliger, D. S., Betlach, M. C., and Stroud, R. M. (1993) *Biochemistry 32*, 1332−1337.
27. Kataoka, M., Kamikubo, H., Tokunaga, F., Brown, L. S., Yamazaki, Y., Maeda, A., Sheves, M., Needleman, R., and Lanyi, J. K. (1994) *J. Mol. Biol. 243*, 621−638.
28. Tittor, J., Soell, C., Oesterhelt, D., Butt, H.-J., and Bamberg, E. (1989) *EMBO J. 8*, 3477−3482.
29. Cao, Y., Váró, G., Chang, M., Ni, B., Needleman, R., and Lanyi, J. K. (1991) *Biochemistry 30*, 10972−10979.
30. Le Coutre, J., Tittor, J., Oesterhelt, D., and Gerwert, K. (1995) *Proc. Natl. Acad. Sci. U.S.A. 92*, 4962−4966.
31. Brown, L. S., and Lanyi, J. K. (1996) *Proc. Natl. Acad. Sci. U.S.A. 93*, 1731−1734.
32. Tittor, J., Wahl, M., Schweiger, U., and Oesterhelt, D. (1994) *Biochim. Biophys. Acta 1187*, 191−197.
33. Brown, L. S., Kamikubo, H., Zimányi, L., Kataoka, M., Tokunaga, F., Verdegem, P., Lugtenburg, J., and Lanyi, J. K. (1997) *Proc. Natl. Acad. Sci. U.S.A. 94*, 5040−5044.
34. Dickopf, S., Alexiev, U., Krebs, M. P., Otto, H., Mollaaghababa, R., Khorana, H. G., and Heyn, M. P. (1995) *Proc. Natl. Acad. Sci. U.S.A. 92*, 11519−11523.
35. Tittor, J., Schweiger, U., Oesterhelt, D., and Bamberg, E. (1994) *Biophys. J. 67*, 1682−1690.
36. Tittor, J., Haupts, U., Haupts, C., Oesterhelt, D., Becker, A., and Bamberg, E. (1997) *J. Mol. Biol. 271*, 405−416.
37. Spudich, J. L., and Lanyi, J. K. (1996) *Curr. Opin. Cell Biol. 8*, 452−457.
38. Grigorieff, N., Ceska, T. A., Downing, K. H., Baldwin, J. M., and Henderson, R. (1996) *J. Mol. Biol. 259*, 393−421.
39. Kimura, Y., Vassylyev, D. G., Miyazawa, A., Kidera, A., Matsushima, M., Mitsuoka, K., Murata, K., Hirai, T., and Fujiyoshi, Y. (1997) *Nature* 389, 206−211.
40. Pebay-Peyroula, E., Rummel, G., Rosenbusch, J. P., and Landau, E. M. (1997) *Science 277*, 1676−1681.
41. Oesterhelt, D., and Stoeckenius, W. (1974) *Methods. Enzymol. 31*, 667−678.
42. Brown, L. S., Váró, G., Needleman, R., and Lanyi, J. K. (1995) *Biophys. J. 69*, 2103−2111.
43. Zimányi, L., Keszthelyi, L., and Lanyi, J. K. (1989) *Biochemistry 28*, 5165−5172.
44. Sharonov, A. Y., Tkachenko, N. V., Savransky, V. V., and Dioumaev, A. K. (1991) *Photochem. Photobiol. 54*, 889−893.
45. Dioumaev, A. K. (1997) *Biophys. Chem. 76*, 1−26.
46. Zimányi, L., and Lanyi, J. K. (1997) *J. Phys. Chem. B 101*, 1930−1933.
47. Sawatzki, J., Fischer, R., Scheer, H., and Siebert, F. (1990) *Proc. Natl. Acad. Sci. U.S.A. 87*, 5903−5906.
48. Smith, S. O., Braiman, M., Myers, A. B., Pardoen, J. A., Courtin, J., Winkel, C., Lugtenburg, J., and Mathies, R. A. (1987a) *J. Am. Chem. Soc. 109*, 3108−3125.
49. Smith, S. O., Pardoen, J. A., Lugtenburg, J., and Mathies, R. A. (1987b) *J. Phys. Chem. 91*, 804−819.
50. Ohtani, H., Kobayashi, T., Iwai, J.-I., and Ikegami, A. (1986) *Biochemistry 25*, 3356−3363.
51. Nilsson, A., Rath, P., Olejnik, J., Coleman, M., and Rothschild, K. J. (1995) *J. Biol. Chem. 270*, 29746−29751.
52. Lanyi, J. K. (1986) *Biochemistry 25*, 6706−6711.
53. Lanyi, J. K., and MacDonald, R. E. (1979) *Methods. Enzymol. 56*, 398−407.

54. Maeda, A. (1995) *Isr. J. Chem. 35*, 387−400.
55. Smith, S. O., Lugtenburg, J., and Mathies, R. A. (1985) *J. Membr. Biol. 85*, 95−109.
56. Orlandi, G., and Schulten, K. (1979) *Chem. Phys. Lett. 64*, 370−374.
57. Tavan, P., Schulten, K., and Oesterhelt, D. (1985) *Biophys. J. 47*, 415−430.
58. Fodor, S. P., Ames, J. B., Gebhard, R., van der Berg, E. M., Stoeckenius, W., Lugtenburg, J., and Mathies, R. A. (1988a) *Biochemistry 27*, 7097−7101.
59. Fodor, S. P., Pollard, W. T., Gebhard, R., van den Berg, E. M., Lugtenburg, J., and Mathies, R. A. (1988b) *Proc. Natl. Acad. Sci. U.S.A. 85*, 2156−2160.
60. Ames, J. B., Fodor, S. P. A., Gebhard, R., Raap, J., van den Berg, M. M., Lugtenburg, J., and Mathies, R. A. (1989) *Biochemistry 28*, 3681−3687.
61. Smith, S. O., Pardoen, J. A., Mulder, P. P. J., Curry, B., Lugtenburg, J., and Mathies, R. A. (1983) *Biochemistry 22*, 6141−6148.
62. Gerwert, K., and Siebert, F. (1986) *EMBO J. 5*, 805−811.
63. Bogomolni, R. A., Stoeckenius, W., Szundi, I., Perozo, E., Olson, K. D., and Spudich, J. L. (1994) *Proc. Natl. Acad. Sci. U.S.A. 91*, 10188−10192.
64. Spudich, J. L. (1994) *Cell 79*, 747−750.
65. Haupts, U., Haupts, C., and Oesterhelt, D. (1995) *Proc. Natl. Acad. Sci. U.S.A. 92*, 3834−3838.
66. Haupts, U., Bamberg, E., and Oesterhelt, D. (1996) *EMBO J. 15*, 1834−1841.
67. Hoff, W. D., Jung, K. H., and Spudich, J. L. (1997) *Annu. Rev. Biophys. Biomol. Struct. 26*, 223−258.
68. Brown, L. S., Needleman, R., and Lanyi, J. K. (1996) *Biochemistry 35*, 16048−16054.
69. Sasaki, J., Brown, L. S., Chon, Y.-S., Kandori, H., Maeda, A., Needleman, R., and Lanyi, J. K. (1995) *Science 269*, 73−75.
70. Váró, G., Zimányi, L., Chang, M., Ni, B., Needleman, R., and Lanyi, J. K. (1992) *Biophys. J. 61*, 820−826.
71. Zimányi, L., Váró, G., Chang, M., Ni, B., Needleman, R., and Lanyi, J. K. (1992) *Biochemistry 31*, 8535−8543.
72. Druckmann, S., Friedman, N., Lanyi, J. K., Needleman, R., Ottolenghi, M., and Sheves, M. (1992) *Photochem. Photobiol. 56*, 1041−1047.
73. Hessling, B., Herbst, J., Rammelsberg, R., and Gerwert, K. (1997) *Biophys. J. 73*, 2071−2080.
74. Dickopf, S., and Heyn, M. P. (1997) *Biophys. J. 73*, 3171−3181.
75. Perkins, G. A., Liu, E., Burkard, F., Berry, E. A., and Glaeser, R. M. (1992) *J. Struct. Biol. 109*, 142−151.
76. Vonck, J., Han, B.-G., Burkard, F., Perkins, G. A., and Glaeser, R. M. (1994) *Biophys. J. 67*, 1173−1178.
77. Han, B.-G., Vonck, J., and Glaeser, R. M. (1994) *Biophys. J. 67*, 1179−1186.
78. Kamikubo, H., Kataoka, M., Váró, G., Oka, T., Tokunaga, F., Needleman, R., and Lanyi, J. K. (1996) *Proc. Natl. Acad. Sci. U.S.A. 93*, 1386-1390.
79. Vonck, J. (1996) *Biochemistry 35*, 5870−5878.
80. Sass, H. J., Schachowa, I. W., Rapp, G., Koch, M. H. J., Oesterhelt, D., Dencher, N. A., and Büldt, G. (1997) *EMBO J. 16*, 1484−1491.
81. Nagle, J. F., and Mille, M. (1981) *J. Chem. Phys. 74*, 1367−1372.
82. Schulten, K., Schulten, Z., and Tavan, P. (1984) in *Information and Energy Transduction in Biological Membranes* (Bolis, A., Helmreich, H., and Passow, H., Eds.) pp 113−131, Alan R. Liss, Inc., New York.
83. Henderson, R., Baldwin, J. M., Ceska, T. A., Zemlin, F., Beckmann, E., and Downing, K. H. (1990) *J. Mol. Biol. 213*, 899−929.
84. Balashov, S. P., Govindjee, R., Imasheva, E. S., Misra, S., Ebrey, T. G., Feng, Y., Crouch, R. K., and Menick, D. R. (1995) *Biochemistry 34*, 8820−8834.
85. Brown, L. S., Gat, Y., Sheves, M., Yamazaki, Y., Maeda, A., Needleman, R., and Lanyi, J. K. (1994) *Biochemistry 33*, 12001−12011.
86. Nagel, G., Kelety, B., Möckel, G., Büldt, G., and Bamberg, E. (1998) *Biophys. J. 74*, 403−412.
87. Humphrey, W., Bamberg, E., and Schulten, K. (1997) *Biophys. J. 72*, 1347−1356.
88. Moltke, S., Krebs, M. P., Mollaaghababa, R., Khorana, H. G., and Heyn, M. P. (1995) *Biophys. J. 69*, 2074−2083.
89. Mowery, P. C., Lozier, R. H., Chae, Q., Tseng, Y. W., Taylor, M., and Stoeckenius, W. (1979) *Biochemistry 18*, 4100−4107.
90. Váró, G., and Lanyi, J. K. (1989) *Biophys. J. 56*, 1143−1151.
91. Renthal, R., Shuler, K., and Regalado, R. (1990) *Biochim. Biophys. Acta 1016*, 378−384.
92. Dér, A., Száraz, S., Tóth-Boconádi, R., Tokaji, Z., Keszthelyi, L., and Stoeckenius, W. (1991) *Proc. Natl. Acad. Sci. U.S.A. 88*, 4751−4755.
93. Marti, T., Otto, H., Rösselet, S. J., Heyn, M. P., and Khorana, H. G. (1992) *J. Biol. Chem. 267*, 16922−16927.
94. Havelka, W. A., Henderson, R., and Oesterhelt, D. (1995) *J. Mol. Biol. 247*, 726−738.
95. Váró, G., Needleman, R., and Lanyi, J. K. (1995) *Biochemistry 34*, 14500−14507.
96. Rousso, I., Friedman, N., Sheves, M., and Ottolenghi, M. (1995) *Biochemistry 34*, 12059−12065.
97. Gat, Y., and Sheves, M. (1993) *J. Am. Chem. Soc. 115*, 3772−3773.
98. Dencher, N. A., Dresselhaus, D., Zaccai, G., and Büldt, G. (1989) *Proc. Natl. Acad. Sci. U.S.A. 86*, 7876−7879.
99. Nakasako, M., Kataoka, M., Amemiya, Y., and Tokunaga, F. (1991) *FEBS Lett. 292*, 73−75.
100. Subramaniam, S., Gerstein, M., Oesterhelt, D., and Henderson, R. (1993) *EMBO J. 12*, 1−8.
101. Thorgeirsson, T. E., Xiao, W., Brown, L. S., Needleman, R., Lanyi, J. K., and Shin, Y.-K. (1997) *J. Mol. Biol. 273*, 951−957.
102. Váró, G., Needleman, R., and Lanyi, J. K. (1996) *Biophys. J. 70*, 461−467.
103. Váró, G., and Lanyi, J. K. (1995) *Biochemistry 34*, 12161−12169.
104. Maeda, A., Kandori, H., Yamazaki, Y., Nishimura, S., Hatanaka, M., Chon, Y. S., Sasaki, J., Needleman, R., and Lanyi, J. K. (1997) *J. Biochem. (Tokyo) 121*, 399−406.

BI9728396